

A Superelastic Retrofitting Method for Mitigating the Effects of Seismic Excitations on Irregular Bridges

Ghassemieh, M.^{1*}, Ghodrati Kashan, S.M.², Khanmohammadi, M.³ and Baei, M.⁴

¹ Professor, School of Civil Engineering, College of Engineering, University of Tehran, Tehran, Iran.

² M.Sc., School of Civil Engineering, College of Engineering, Sharif University, Tehran, Iran.

³ Assistant Professor, School of Civil Engineering, College of Engineering, University of Tehran, Tehran, Iran.

⁴ M.Sc., School of Civil Engineering, College of Engineering, University of Tehran, Tehran, Iran.

Received: 06 Sep. 2017;

Revised: 27 Feb. 2018;

Accepted: 13 Mar. 2018

ABSTRACT: Irregularities in bridge pier stiffness concentrate the ductility demand on short piers; while not operating on the longer and more flexible ones. The existence of non-uniform, ductility demand distribution in bridges significantly influences seismic response. As such, this paper proposes a new approach for balancing the ductility demand in irregular bridges by utilizing Shape Memory Alloys (SMAs). An irregular, single column bent viaduct with unequal pier heights is modeled and used as a reference bridge. To enhance seismic behavior of the bridge, a fixed bearing at the top of the short pier is replaced by a sliding bearing and two groups of SMA bars. SMAs are designed to keep their maximum strain within the super-elastic range. The seismic response of the controlled bridge is compared with a reference bridge through parametric studies using a set of suitable ground motion records. Study parameters include SMA lengths, short pier reinforcement ratios, design strain of SMA elements, and the heights of the medium and long piers. The proposed method successfully reduced the response of the short pier and, hence, improved the overall seismic behavior.

Keywords: Bridge, Ductility Demand, Energy Dissipation, Irregularity, Seismic Response, Shape Memory Alloy (SMA).

INTRODUCTION

During and after seismic events, bridges are critical for evacuation and reconstruction activities. As reported by many researchers the poor performance of bridges in past earthquakes has highlighted the need for improved seismic performance. This includes

developing and deploying new aseismic designs and devices. Although current, force-based design procedures (which are based on initial stiffness) are applicable to a wide range of regular structures, they have not to date proved to be reliable in predicting the seismic behavior of irregular structures. Hence, bridge design specifications usually tie force-

* Corresponding author E-mail: mghassem@ut.ac.ir

based design to satisfy regularity requirements. Table 1 presents the regularity bridge requirements in the AASHTO specifications (AASHTO, 2007). Due to rough topography of mountain valleys or urban transportation constraints, the regularity requirements of Table 1 may be unachievable, thereby resulting in the construction of irregular bridges due to unequal column heights and/or different span lengths. Irregularities in the stiffness of adjacent piers lead to concentrations of seismic shear force and higher ductility demands on stiffer (shorter) piers. Balancing the stiffness of piers by changing their cross-sectional dimensions is often not an acceptable solution due to architectural considerations. Hence, designers sometimes use other techniques for balancing the stiffness of adjacent bents. As suggested by the Federation Internationale du Beton (FIB, 2007), these may include ‘pre-shafts’ (upward extensions of the foundation shaft) that increase the effective height of shorter piers, combinations of monolithic and bearing deck-pier connections, or adjustments in the stiffness characteristics of the bearings placed at specific bents. While these generate more balanced stiffness of adjacent bents, they often increase the natural period and, consequently, exacerbate bridge deck displacement demands. Such demands in turn require a bearing with high displacement capacity, which is expensive and may still not meet the needs of bridges with high natural periods. Thus, further research for improving the seismic behavior of irregular bridges is required. To address the current shortcomings, a new retrofit

approach using a shape memory alloy (SMA) bars is proposed.

SHAPE MEMORY ALLOY

Shape memory alloys are a relatively new class of metallic alloys that exhibit unique characteristics, based on solid-solid martensitic phase transformation (Sharabash and Andrawes, 2009). Among them, Nitinol SMAs possess several characteristics that make them attractive for retrofitting, particularly bridges. These characteristics include the following: 1) large elastic strain ranges; 2) hysteretic damping; 3) reliable energy dissipation through repeated solid-state phase transformation; 4) strain hardening at strains above 6%; 5) excellent low- and high-cycle fatigue properties; 6) exceptional corrosion resistance; and 7) stress plateau formation during phase transformation, which controls the forces transmitted to the structure as reported (Sharabash and Andrawes, 2009). An SMA can be categorized as either super-elastic austenite (high temperature phase), which recovers its original shape when unloaded or martensite (low temperature phase), which exhibits shape memory effects only recovering its original shape when heated. Figure 1 show a schematic of the stress-strain relationship typically observed in super-elastic and martensitic SMAs, respectively. The super-elastic SMA possesses a flag-shaped hysteresis with a zero residual strain, while the martensitic SMA is characterized by a relatively low stress plateau and non-zero, residual strains. The study herein will concentrate on the former SMA type.

Table 1. Regular bridge requirements

Parameter	Value				
Number of spans \Rightarrow	2	3	4	5	6
Maximum span length ratio (span to span)	3	2	2	1.5	1.5
Maximum pier stiffness ratio (span to span)	-	4	4	3	2

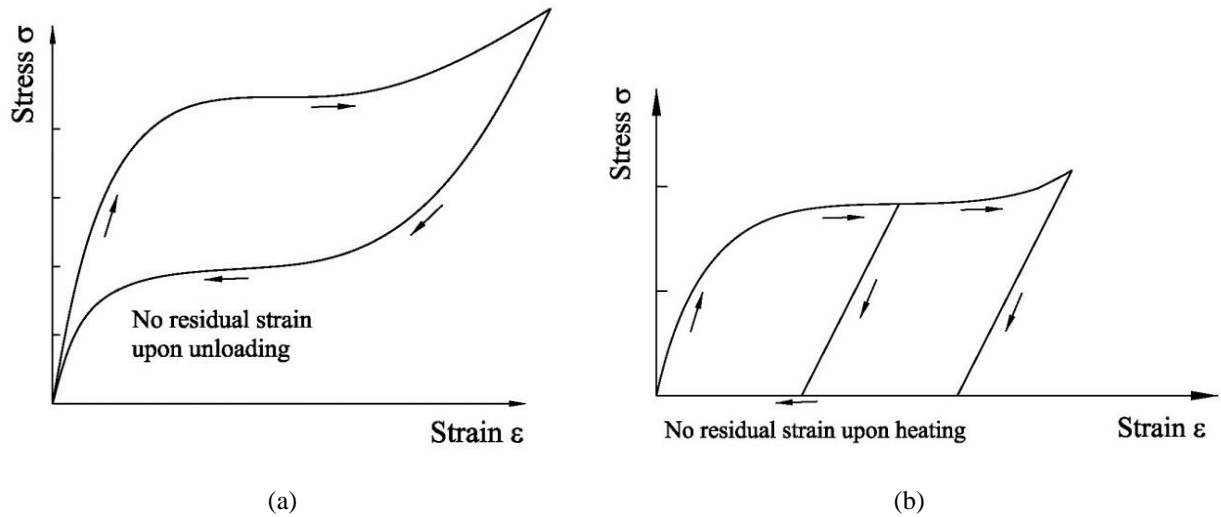


Fig. 1. Stress-strain diagrams: a) Super-elastic behavior, b) Shape memory effect

It has been shown in the recent earthquakes, many bridges with steel restrainer experienced severe damage. Bridges that had been designed or retrofitted with restrainer cables or steel bars failed in both the Loma Prieta and Northridge earthquakes. Also many Japanese restraining bars had a disappointing behavior during the Kobe earthquake. In addition, it has been demonstrated that steel restrainers do not dissipate much amount of energy, since they are usually intended to remain elastic. It has also been demonstrated that a large number of steel restrainers is often required for the bridges to limit lateral movement to acceptable levels. In those circumstances, extra number of restrainers would induce large forces in other components of the bridge. Therefore, the weakness of steel restrainers can technically be addressed by utilizing the shape memory alloy bars.

Several studies have evaluated the feasibility of using SMAs for bridge structures. Due to re-centering and energy dissipating capabilities of SMAs, many researchers have considered SMA devices as restrainers for seismic protection of bridges (Johnson et al., 2008; Guo et al., 2012). In such studies, the SMA restrainers were shown to be very effective in preventing

unseating and seismic-induced pounding. Specifically in another study (Sharabash and Andrawes, 2009) explored the use of SMA dampers for seismic control of cable-stayed bridges. The results showed that SMA dampers were able to reduce the bridge response significantly. In another study (Han et al., 2006) the researchers utilized NiTi SMA wires to simultaneously damp tension, compression and torsion, in an arrangement developed for structural control implementation. The mechanical analysis of the NiTi-wire SMA dampers was done based on a model of the SMA-wire restoring force and on tension-compression and torsion damping analyses. The analytical damping results were found to be similar to those generated experimentally.

Significant work has also been done with respect to SMA Niti bars (Ghassemieh et al. 2012a,b; Ghassemieh et al. 2013; Farmani and Ghassemieh, 2016; Farmani and Ghassemieh, 2017; Ghassemieh et al., 2017); in which the seismic enhancement of the concrete or steel structures are achieved by utilizing such bars. Also in the study done by (Shrestha et al., 2011), the applicability of developed Cu-Al-Mn SMA bars for retrofitting of historical masonry constructions was performed. Experimental

and numerical outcomes in that work showed the superiority of Cu-Al-Mn SMA bars compared to conventional steel reinforcing bars in the retrofitting of historical masonry. In related work (Saiidi and Wang, 2006) the idea of SMA bars instead of steel bars in the plastic hinge zone of reinforced concrete bridge piers was presented; while the cyclic behavior of post-tensioned segmental bridge columns tied with SMA link-bars was examined by other researchers (Roh et al., 2012).

Work has also been conducted to look at SMA isolation systems. For example, the efficiency of an SMA as an isolation system component was demonstrated (Alvandi and Ghassemieh, 2014). They concluded that an SMA isolation system can enhance the behavior in terms of response reduction and recentering performance. Seismic performance of rubber-based, as well as sliding-type base, isolation systems equipped with a Nitinol shape memory alloy device with consideration of the effects of environmental temperature changes was evaluated (Ozbulut and Hurlebaus, 2011). The authors concluded that temperature has only a limited effect on the performance of bridges isolated with the proposed SMA-based isolation system. More recently, (Aryan and Ghassemieh, 2014, 2015, 2017) vertical component of seismic excitations which is affected on the performance of bridges during the earthquakes were evaluated. They evaluated a superelastic based system for designing as well as retrofitting the multi span bridges. The study showed the efficiency of the new system subjected to the vertical and horizontal seismic excitations is confirmed according to reduction of the bridge responses and improvement in nonlinear performance of the columns in comparison with the as-built bridge results. Notably, these studies all focused on regularly shaped bridges.

Given these previous successes, the

following research investigates the applicability of using Nitinol shape memory alloy for balancing the energy and ductility demands in irregular bridges.

ANALYTICAL MODEL

Proposed Retrofitting Technique

To improve seismic behavior, what is proposed is the replacement of the fixed bearing at the top of each short pier by a sliding bearing plus two groups of SMA bars that connect the pier cap to the girder bottom (Figure 2). These connecting bars would provide a relatively simple alternative to using a tension-compression device. The two groups of SMA elements would work alternately in the positive and negative longitudinal directions and, thereby, act only in tension. The two elements are assumed to be identical in their mechanical properties and to behave symmetrically under loading reversal. The sliding bearing has a very small horizontal stiffness, and for simplicity, its stiffness is taken to be zero in this study, as it is considered to have only a negligible effect on the global response.

The SMA material model in the OpenSees (McKenna, 2011) material library is used to describe the analytical model of the SMA devices. This uniaxial, tension-only model is capable of describing the constitutive behavior of super-elastic SMAs at a constant temperature. The analytical model of the SMA material is presented in Figure 3. The model requires six material parameters: 1) Young's modulus of austenite (E_A); 2) the austenite-to-martensite phase transformation starting yield stress (σ_{am-s}); 3) transformation strain hardening (α); 4) a strain value at the end of the phase transformation (ε_L); 5) the martensite-to-austenite phase transformation starting stress (σ_{ma-s}); and 6) the stress level at which the martensite-to-austenite phase transformation finishes (σ_{ma-f}).

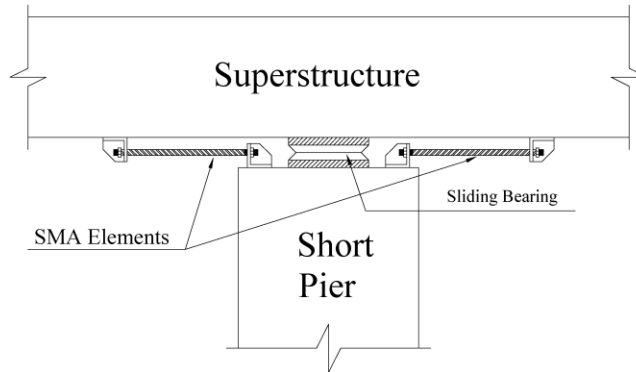


Fig. 2. Schematic of the setup proposed for SMA elements and a sliding bearing

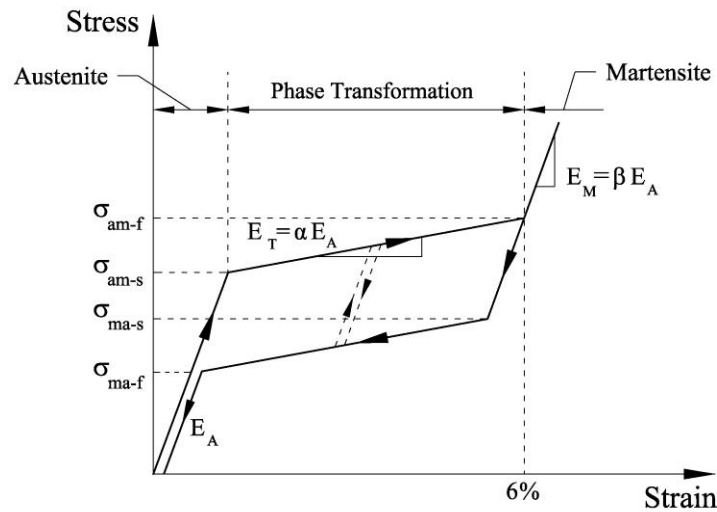


Fig. 3. Stress-strain relationship of the super-elastic SMA material

The SMA model represents an idealized one-dimensional behavior for SMA material where no strength degradation occurs during cycling, and the residual deformation is taken as zero at the end of each cycle. There is a further assumption that austenite and martensite branches have the same modulus of elasticity ($\beta = 1$). In this study, the strain

value at the end of the phase transformation is set at 6%, as is typical for a super-elastic SMA, and the recoverable elongation is taken as 8%. Other SMA material parameters that were considered are presented in Table 2. The SMA elements are modeled with a truss element available in the OpenSees software.

Table 2. SMA mechanical properties Brocca et al. (2002)

Parameter	Value
E_A	60 GPa
σ_{am-s}	420 MPa
α	0.05
ϵ_L	6 %
σ_{ma-s}	300 MPa
σ_{ma-f}	140 MPa

Design of SMA Devices

A certain amount of trial and error is usually required for selecting design parameters of SMA devices since their geometry can change the dynamic characteristics of the bridge structure. One main concern is keeping the maximum strain of the SMA elements within the recoverable strain range (up to 6%-8%) during strong ground motions. This objective may require long SMA devices, which have the disadvantage of decreasing the structure's stiffness and increasing the displacement demand, as well as increasing the total volume of the SMA material required.

In this study, the cross-sectional areas of the SMA devices are designed to limit the maximum strain of SMA elements to the super-elastic strain range. To do so, the plastic shear strength of short columns with different longitudinal reinforcement ratios (ρ) are set equal to the axial strength of the SMA elements at 6% strain. In other words, when the SMA elements reach a strain of 6%, the short column is intended to yield. Therefore the developed forces in the SMA elements are controlled. Hence, the SMA devices do not experience strains beyond ultimate design strain of 6%. Table 3 presents the short pier plastic shear strength and cross-sectional area of SMA devices for different short pier reinforcement ratios. This design philosophy assures that the super-elasticity feature of the SMAs is retained, even under severe earthquakes.

REFERENCE BRIDGE

A reference bridge is used herein to demonstrate the value of the proposed approach. The bridge is of reinforced concrete and consists of a single column bent viaduct, which was designed and investigated as part of the research program in support of the Eurocode provision for the definition of irregularity and design procedures for

irregular bridges (Calvi and Pinto, 1994) and is widely used as a benchmark reference bridge (e.g. Kappos et al., 2002; Isakovic and Fischinger, 2006; Pinto et al., 1996; Isakovic et al., 2008). The bridge has a 200 m long continuous deck divided into four equal spans. The boxed section deck has a 14 m width and is supported by abutments and 3 intermediate piers of unequal heights (14 m, 7 m, and 21 m). Each pier has a hollow rectangular section with a longitudinal reinforcement ratio (ρ) of 1.0% and a transverse reinforcement ratio of 0.9%. Figure 4 presents details of the deck and pier cross-sections. This study employs the material characteristics adopted by (Pinto et al., 1996): concrete compressive strength of 35 MPa and pier reinforcing bars yield strength of 500 MPa and Young's modulus of 201 GPa. The pier stiffness ratio between the medium and short piers and the short and long piers are 8 and 27, respectively. Hence, based on the AASHTO Specifications, which proposes a pier stiffness ratio of 4 as a regularity limit for a four-span bridge, the reference bridge is considered to be irregular.

Analytical Model of the Reference Bridge

A two-dimensional (2D) finite element model of the reference bridge and of the SMA retrofitted bridge were developed and analyzed using the open-source, OpenSees finite element program (McKenna, 2011). The bridge deck was modeled using 40 elastic, beam-column elements with 41 nodes. Columns in the plastic hinge zone were modeled using nonlinear, beam-column elements with distributed plasticity and material behaviors. A fiber-based model was employed using a uniaxial stress-strain relationship to represent the confined and unconfined concrete and the longitudinal reinforcing steel.

The deck-to-pier connections were idealized with fixed bearings; assuming the deck to be longitudinally free at the

abutments. For regions beyond the plastic hinge zones, the columns were modeled with an elastic, beam-column element. The mass of the deck and piers were lumped at the nodes. The fixed bearings were modeled by zero length elements. The damping matrix of the substructure was computed by the Rayleigh method, and a damping ratio (ξ) of 3% was chosen for the 2 effective natural frequencies of the bridge in the longitudinal direction. In addition, to obtain an accurate value of the moments at each column base, rigid links were used to level the center of the mass in the reference bridge of the analytical model. Figure 5 illustrates the schematic of model in the OpenSees program environment. According to the results obtained from the eigenvalue analysis, the predominant natural period of the bridge in the longitudinal direction is about 1.17 seconds.

Pushover Analysis on the Reference Bridge

To investigate the seismic behavior of the reference bridge, a non-linear static (pushover) analysis was conducted in the longitudinal direction. Figure 6a presents the pushover curves (base shear versus piers top displacement) up to the displacement capacity of the short pier (i.e. 350 mm). Irregularities in pier height and stiffness caused a severe concentration of the ductility demand (μ) on the stiffer, short pier. As shown in Figure 6b, while the short pier experienced a ductility demand of 7.0, the medium and long piers only experienced ductility demands of 3.5 and 2.3, respectively.

GROUND MOTIONS

A set of 10 far-field ground motion records were selected from the PEER near-ground acceleration (NGA) database (Baker, 2011) according to recommendations made by

FEMA (FEMA, 2009). The records had magnitudes and peak ground accelerations (PGAs) greater than 6.5 and 0.2g, respectively. Table 4 characterizes the ground motions used in the analyses. The records were scaled to an AASHTO specifications design response spectrum between periods of 0.2 T to 1.5 T; in which T was the fundamental period of the bridge. An AASHTO specification design response spectrum was developed using the 10% probability of exceedance in 50 years, the seismic hazard maps with soil profile Type 2, and an acceleration coefficient of 0.35 g. Figure 7 shows a comparison between the code-based design response spectrum and the average response spectrum of the 10 ground motion records, after they were scaled.

EVALUATION CRITERIA

For finding a quantitative comparison basis between the retrofitted bridge and the reference bridge, appropriate structural indicators were required. These indicators are related to ductility demand, damage indices, and the SMA energy dissipation capacity parameters, which are presented in a normalized format relative to the reference bridge response.

Ductility Demand

One of the main objectives of this study is to evaluate the effect of the proposed retrofitting method on the ductility demand of different piers in the SMA-controlled bridge, in comparison to the reference bridge. So the first evaluation criterion being the ductility demand ratio (DDR) is defined according to Eq. (1):

$$DDR = \frac{\mu_{\text{retrofitted}}}{\mu_{\text{reference}}} \quad (1)$$

in which $\mu_{\text{retrofitted}}$ and $\mu_{\text{reference}}$: are the ductility demand of piers in the retrofitted bridge and the reference bridge, respectively.

Table 3. SMA cross-sectional area for different short pier reinforcement ratios

Type	Reinforcement Percent Ratio (ρ)	Plastic Shear Strength (kN)	Cross Sectional Area (mm ²)
P1	1.00	4000	6648
P2	2.00	6000	10029
P3	3.00	8000	13478
P4	4.00	10000	16742

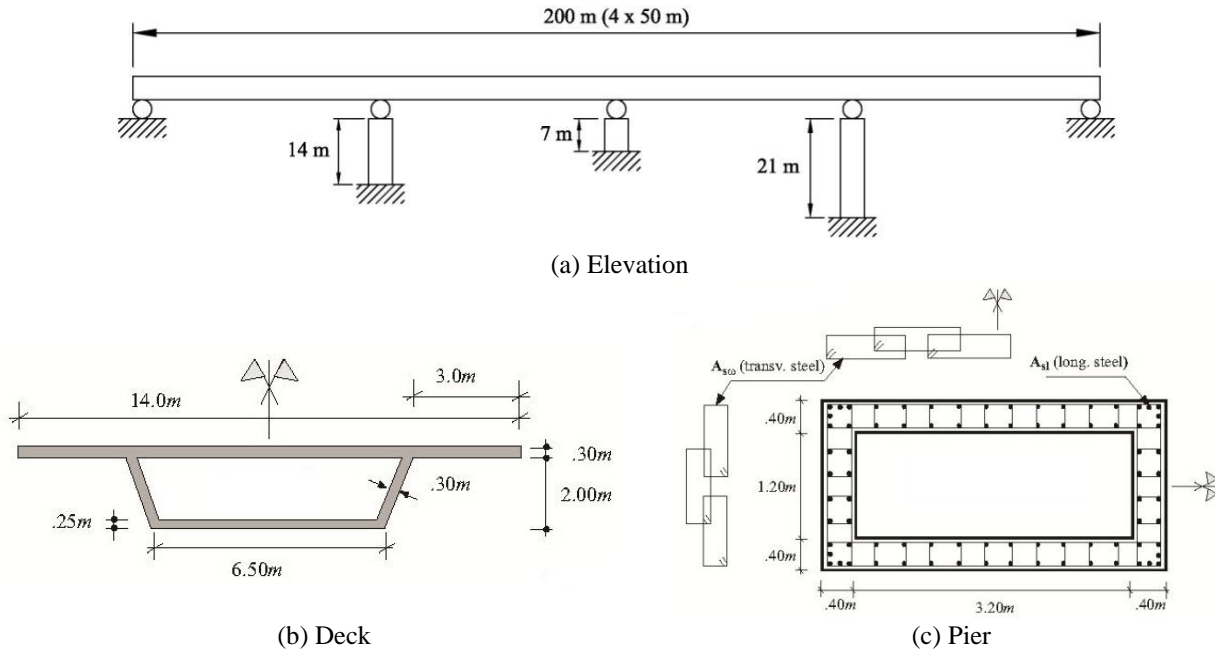


Fig. 4. Reference bridge configuration

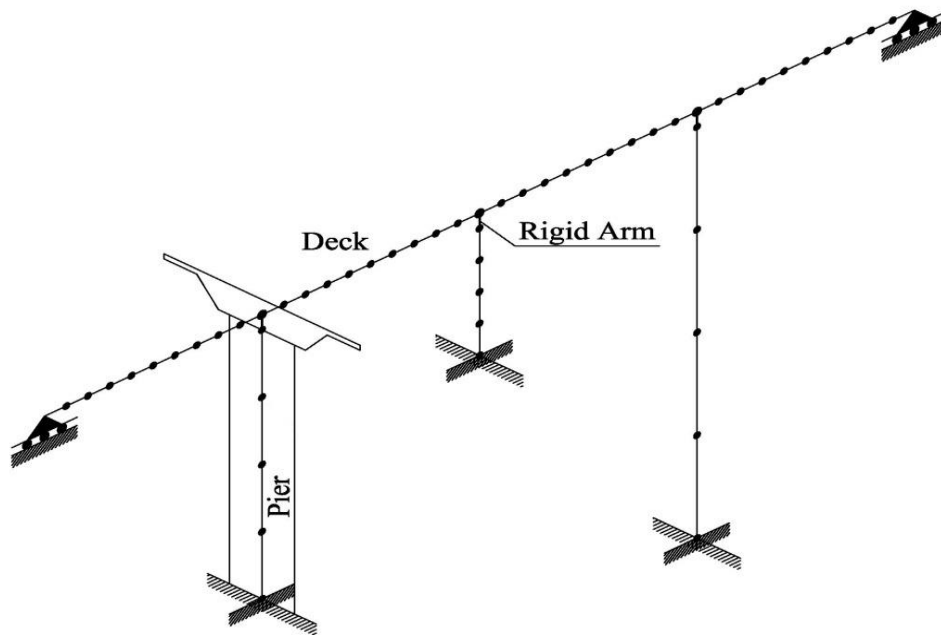


Fig. 5. Analytical model of the reference bridge in OpenSees software

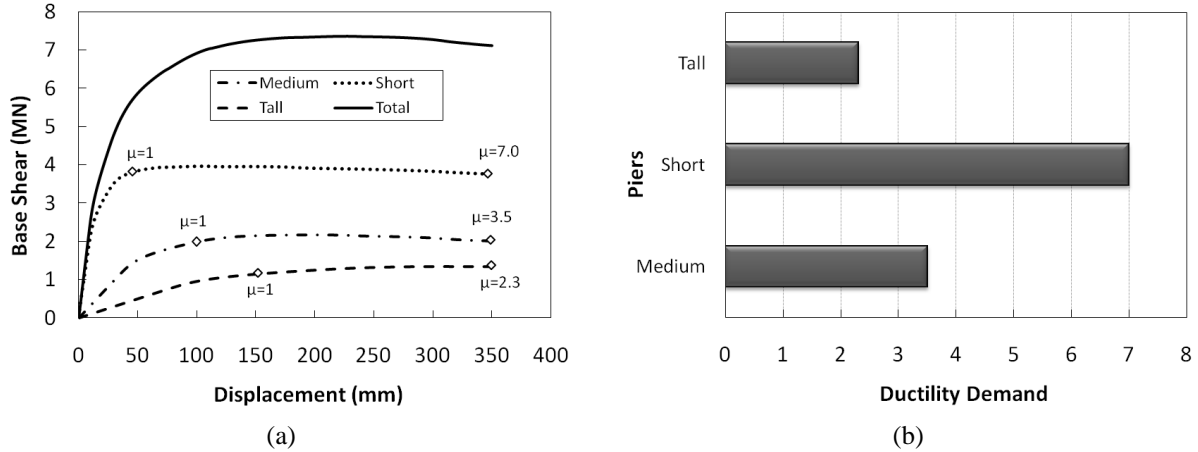


Fig. 6. Pushover Analysis for the reference bridge: a) Pushover curves, b) Ductility demand of different piers

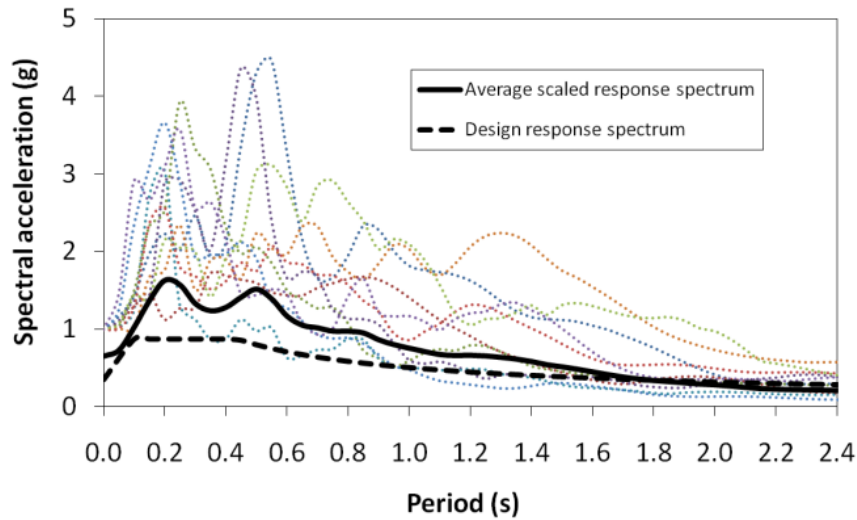


Fig. 7. Employed design response spectrum and the scaled response spectra of the suite of ground motions

Table 4. Descriptions of ground motions used in the analyses

No.	Earthquake	Station	Year	Magnitude	Duration (s)	PGA (g)	PGV (cm/s)
1	Northridge	Beverly Hills - Mulhol	1994	6.7	30	0.517	63
2	Duzce	Bolu	1999	7.1	56	0.822	62
3	Imperial Valley	El Centro Array #11	1979	6.5	39	0.380	42
4	Kobe	Nishi-Akashi	1995	6.9	41	0.509	37
5	Kocaeli	Arcelik	1999	7.5	30	0.218	40
6	Landers	Yermo Fire Station	1992	7.3	44	0.245	52
7	Loma Prieta	Gilroy Array #3	1989	6.9	40	0.555	45
8	Superstition Hills	El Centro Imp. Co	1987	6.5	40	0.358	46
9	Chi-Chi	CHY036	1999	7.6	90	0.294	39
10	San Fernando	LA - Hollywood Stor	1971	6.6	28	0.210	19

Damage Index

Structural performance and damage limit states can be quantified by damage indices. The most widely adopted damage index which is used herein and defined as the

combination of the maximum deformation and hysteretic energy (Eq. (2)):

$$DI = \frac{\delta_m}{\delta_u} + \frac{\beta}{Q_y \delta_u} \int dE \quad (2)$$

where δ_m : is the maximum displacement, δ_u : is the ultimate displacement under monotonic loading, β : is a constant parameter used to characterize the contribution level of the energy demand to the damage, Q_y : is the yield strength and $\int dE$: is the dissipated hysteretic energy. This damage index is valid for an element at the local level. However, the index can be modified to reflect the damage of the entire structure by summing the damage indices, as proposed by Motahari et al. (2007), as per Eq. (3):

$$DI_{\text{Bridge}} = \sum_{i=1}^m \lambda_i DI_i, \quad \lambda_i = \frac{E_i}{\sum_{j=1}^m E_j} \quad (3)$$

in which DI_{Bridge} : is the overall damage index of the bridge, DI_i : is the damage index of the i-th element, m : is the number of elements, E_i : is the hysteretic energy of the i-th element and $\sum_{j=1}^m E_j$: is the total hysteretic energy.

To facilitate direct comparison between the retrofitted and the reference bridges, the ratio of damage indices at the local and global levels is defined as per Eqs. (4-5):

$$DIR = \frac{DI_{\text{retrofitted}}}{DI_{\text{reference}}} \quad (4)$$

$$BDIR = \frac{DI_{\text{retrofitted, bridge}}}{DI_{\text{reference, bridge}}} \quad (5)$$

in which $DI_{\text{retrofitted}}$ and $DI_{\text{reference}}$: are the damage indices at the element level and $DI_{\text{retrofitted, bridge}}$ and $DI_{\text{reference, bridge}}$: are the overall damage indices of the retrofitted and the reference bridge, respectively.

Notably the damage level of the SMA devices is considered to be zero, because of their high fatigue resistance, as suggested by Motahari et al. (2007). This characteristic

seems to be one of the appealing features of this material in decreasing the damage across the entire structure, since the material sustains only insignificant damage, even after a long duration earthquake.

SMA Energy Dissipation Capacity

In the stress-strain diagram typically observed in super-elastic SMAs, the loading and unloading paths do not coincide; the unloading path has a lower stress plateau. As a result, there is an area enclosed under the “flag shape” hysteresis loop, which represents the dissipated energy. Due to excellent low- and high-cycle fatigue properties, SMAs can provide reliable energy dissipation capacity based on a repeatable, solid state phase transformation. In order to assess the capability of SMA devices in dissipating energy, an evaluation criterion is proposed. This is the SMA energy dissipation ratio (SEDR), as defined as per Eq. (6):

$$SEDR = \frac{E_{\text{SMA}}}{E_{\text{tot}}} \quad (6)$$

where E_{SMA} : is the energy dissipated by SMA devices, and E_{tot} : is the total hysteretic energy of the structure.

PARAMETRIC STUDY

The effectiveness of the retrofitting technique in enhancement of irregular bridge behavior is evaluated through a parametric study. For all records, analyses are performed for the as-built bridge, as well as the same bridge equipped with SMA devices. The reinforcement ratios of the short pier, height of the medium and tall piers (degree of irregularity), SMA element lengths, and SMA cross-section areas were investigated with respect to the ultimate SMA device strain levels. Increasing the ultimate SMA device strain levels corresponds to pushing the SMA devices beyond the phase

transformation zone into a strain level of 6.5% and 7% (rather than 6%), in the second strain hardening branch.

Effect of Length of SMA Device

Figures 8 and 9 show the variation of the peak quantities of ductility demand ratio (DDR) and damage index ratio (DIR), respectively, with the length of the SMA device (L_{SMA}) for the short and medium piers under different ground motions. The results were obtained for $\rho = 1\%$ for all piers. Since the medium and long piers had equal top displacements in both the retrofitted and the reference bridge, the DDR of both piers are identical, and the DIRs have the same trend. Therefore, just the response quantities of the medium pier are depicted in Figures 8 and 9. For most cases, the DDR and DIR of the short pier decrease with increasing values of L_{SMA} in the range of 1500 to 3000 mm. Yet, the rate noticeably slows when the L_{SMA} exceeds 2500 mm. By contrast, the ductility demand and damage index of the medium pier increase slightly for greater SMA lengths. Specifically, the average DDR value decreases from 0.58 to 0.42 for the short pier, while that of the medium pier increases from 1.06 to 1.14 when the SMA device length is changed from 1500 to 3000 mm. Similarly, the average short pier DIR decreased from 0.52 to 0.35, while that of the medium pier increased from 1.08 to 1.17 with an increasing L_{SMA} .

Decreasing the ductility demand and damage of the short pier at the expense of an increase in the medium and long piers helps balance the ductility and energy demand on all piers and leads to an overall improvement of irregular bridge behavior, as shown in the bridge damage index ratio (BDIR) and SMA energy dissipation ratio (SEDR), as presented in Figure 10. The Damage Index of the entire bridge, which is calculated based on the method proposed (Motahari et al., 2007) decreases for increasing values of L_{SMA} .

Thus, longer SMA elements possess higher energy dissipation capacities. In particular, when the L_{SMA} is increased from 1500 to 3000 mm, the BDIR decreases on average from 0.53 to 0.43, and the average value of SEDR increases from 0.37 to 0.47.

Notably the BDIR is about the same for an L_{SMA} of 2500 mm as that of 3000 mm. Therefore, an optimum length of the SMA device in this parametric study could be considered as 2500 mm, since little benefit is gained beyond this length. For an $L_{SMA}=2500$ mm, the SMA devices are able to reduce the ductility demand and damage index of the short pier by 56% and 63%, respectively, while there are only 11% and 15% increases in the ductility demand and damage index of the medium pier, respectively. These improvements lead to an overall 55% reduction in the bridge damage index compared to that of the reference bridge.

Effect of the Short Pier Reinforcement

The variation of the peak response quantities with the short pier reinforcement ratios (ρ) is given in Figures 11 and 12 for $L_{SMA} = 2500$ mm. With the SMA devices, different reinforcement ratios of the short piers correspond to different cross-sectional areas of the SMA elements. The results show that while the effect of short pier reinforcement quantities on ductility demand ratio and damage index ratio varies in each record, the mean value responses do not change significantly, and that in the case of $\rho = 2\%$, the SMA devices are more effective in reducing the response of the structure than other reinforcement ratios.

Figures 13a,b compare the short pier and bridge damage index ratio mean responses, for different short pier reinforcement ratios as a function of L_{SMA} subjected to 10 ground motion records. Evaluation of interaction between different values of ρ and L_{SMA} shows that the responses of the bridge are more sensitive to the length of the SMA devices

than the reinforcement ratio. Specifically, in the case of $\rho = 2\%$, BDIR responses are 0.51 and 0.35 for $L_{SMA} = 1500$ and 3000 mm, respectively translating to a 16% reduction in

the damage index of the bridge. However in the case of $L_{SMA} = 2500$ mm, the maximum variation of the bridge damage index differs by only 6% for changes in ρ .

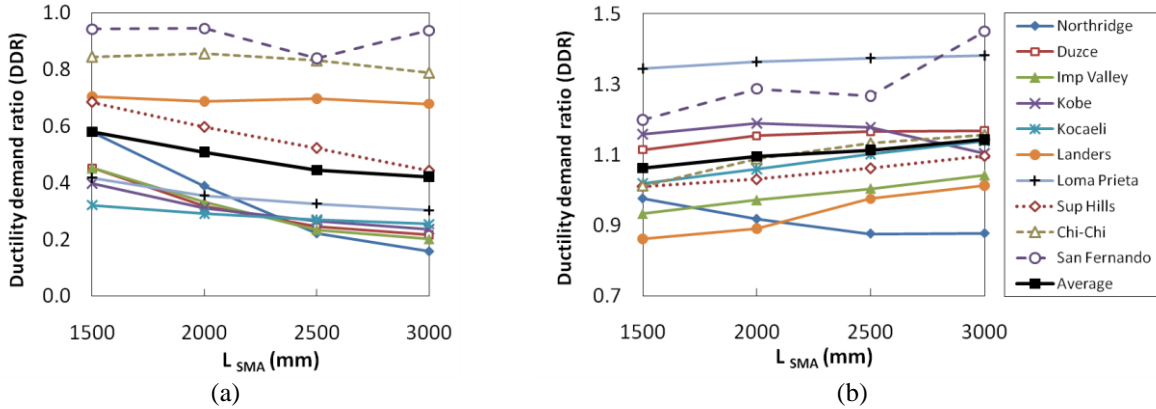


Fig. 8. Ductility demand ratio of the short and medium piers with various lengths of SMA elements: a) Short pier, b) Medium pier

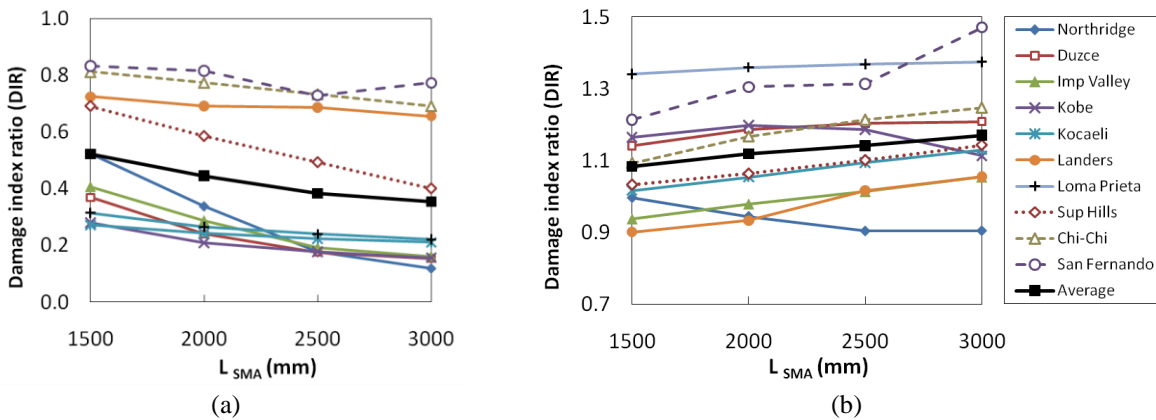


Fig. 9. Damage index ratio of the short and medium piers with different lengths of SMA elements: a) Short pier, b) Medium pier

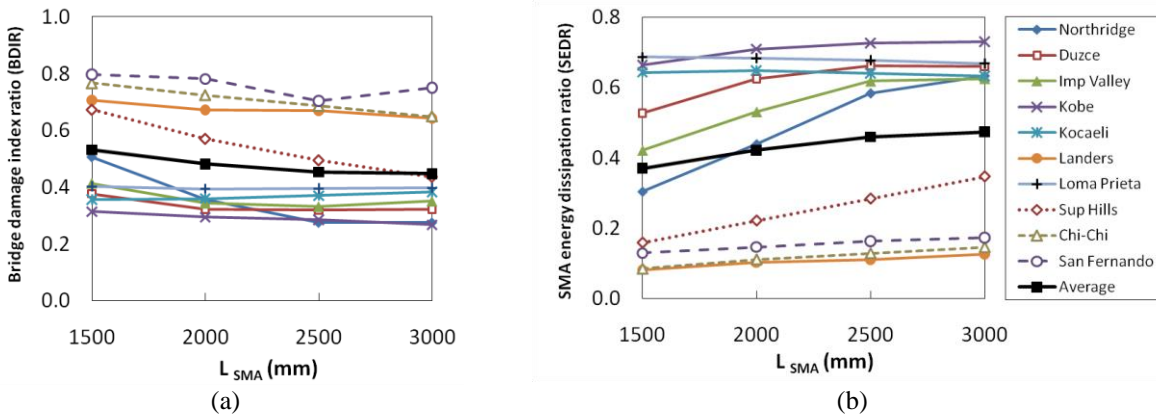


Fig. 10. Bridge damage index ratio and SMA energy dissipation ratio with different lengths of SMA elements: a) Short pier, b) Medium pier

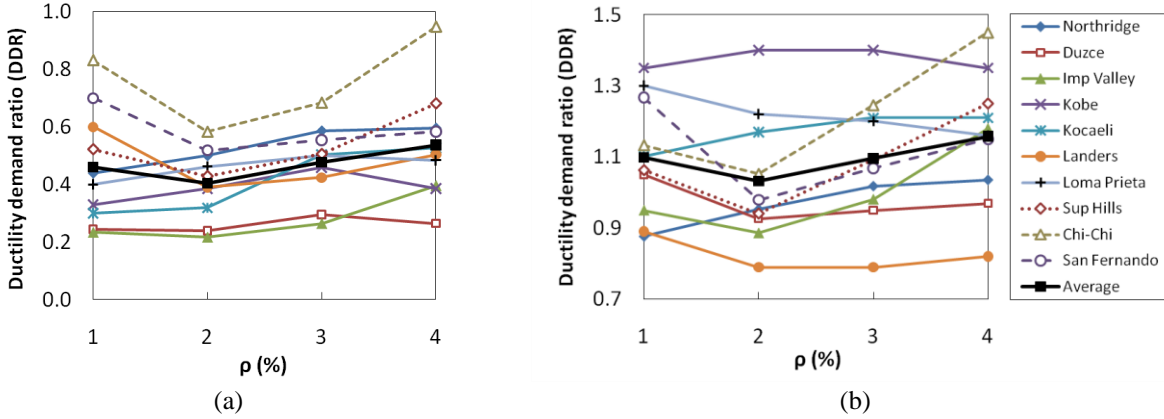


Fig. 11. Ductility demand ratio of the short and medium piers with different short pier reinforcement ratio: a) Short pier, b) Medium pier

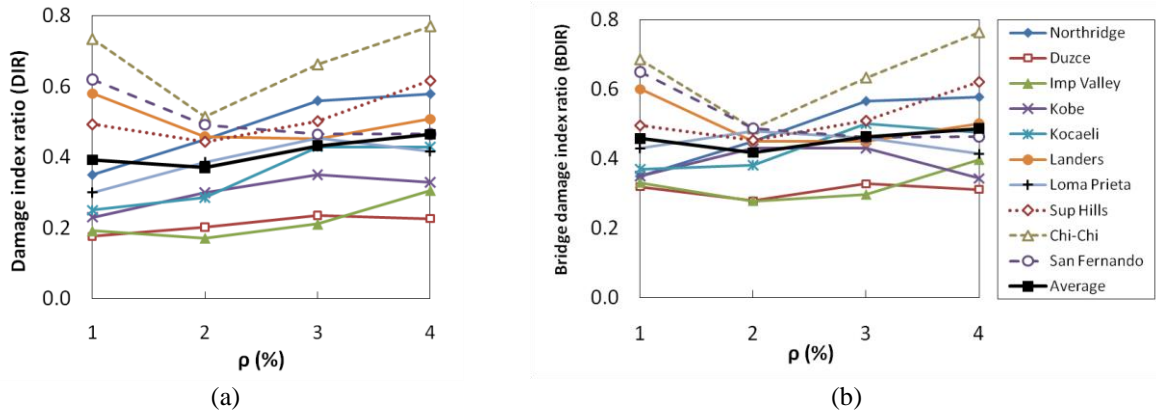


Fig. 12. Damage index ratio with different short pier reinforcement ratio: a) Short pier, b) Entire bridge

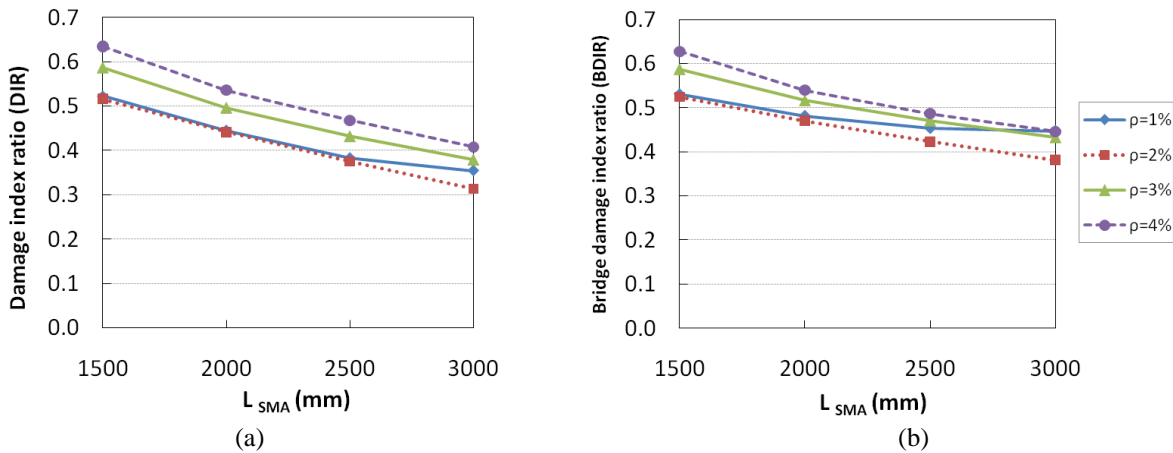


Fig. 13. Variation of the damage index ratio for different values of ρ and L_{SMA} : a) Short pier, b) Entire bridge

Effect of the SMA Design Ultimate Strain

The effect of the design ultimate strain of the SMA elements is investigated by modifying the design procedure. The cross-sectional area of the SMA elements is

designed such that the maximum strain of the SMA bars do not exceed 6% (i.e. the SMA elements do not experience strain hardening). Increasing the design ultimate strain corresponds to a decrease in the cross-

sectional area of the SMA devices and, hence, leads to a reduction in the SMA material (and affiliated cost) used in the retrofitting. Table 5 presents the ultimate design strain and cross-sectional areas of the SMA devices for each procedure. In practical cases, due to strain hardening of pier materials, an increase in the plastic shear strength of the short pier is expected. Thus, strain in the SMA elements may exceed the pre-established functional strain (i.e. 6%). Hence, in the research presented herein, effects of a higher level of SMA design strain on the bridge behavior are examined.

Figures 14 and 15 illustrate the excitations, ductility demand ratio, and damage index ratio of the short pier, respectively, for different design procedures subjected to various earthquakes for $L_{SMA} = 2500$ mm and $\rho = 2\%$. The average results for these are also presented in the same figures. For the Northridge, Duzce, Kocaeli and Loma Prieta records, design procedure 2 (D2) and design procedure 3 (D3), which correspond to SMA design ultimate strain of 6.5% and 7.0%, respectively, have better performance in limiting the ductility demand and damage of the short pier than design procedure 1 (D1), which corresponds to SMA design ultimate strain of 6.0%. However, for other records, the results are comparable between design procedures. In particular, the mean values of the short pier DDR varies between 0.33 and 0.41, and for the DIR between 0.26 and 0.37. Figure 16 also presents the bridge damage index ratio under the considered ground motions. For most excitation cases, each design procedure's outcomes are similar. The performance similarities of variously sized SMA devices are most likely attributable to the fact that for larger strain values, the SMA device has a significant increase in stiffness due to strain hardening, which can compensate for the reduction in elastic stiffness but, consequently, limits the deck displacement.

To provide a better understanding of the mechanical behavior of the SMA devices under the various design procedures, the force-displacement relationship of the SMA elements for the Superstition Hills earthquake, as well as the design ultimate strain of 6% and 7%, are presented in Figure 17. The maximum force in each of the SMA elements approximately equals 6000 KN for both design procedures due to the fact that the cross-sectional area of the SMA devices is devised to balance the axial strength of the SMA elements at design ultimate strain against that of the plastic shear strength of the short pier with a $\rho = 2\%$ (6 MN).

Effect of the Extents of Irregularity

Finally, the effectiveness of the SMA devices for bridge with different degrees of irregularity is investigated. The reference bridge has 3 intermediate piers with medium pier of 14 m in the left, short pier of 7 m in the middle, and tall pier of 21 m in the right (Figure 4). Therefore, the reference bridge has a pier stiffness ratio of 8 between the left and middle piers and of 27 between the middle and right piers, respectively. Two new bridge configurations are developed by changing the height of the medium and tall piers. One case is less irregular than the reference bridge and the other more so. The less irregular bridge has a pair of 14 m piers flanking the 7 m middle pier resulting in stiffness ratios of 8 when comparing an adjacent pier to the middle one. The second bridge has a pair of 21 m piers on the left and right and a 7 m pier in the middle with both stiffness ratios of the adjacent piers equal to 27. This results in a more irregular configuration than the reference bridge.

For simplicity in referring to bridges with different configurations, a geometric label is introduced in the form of BLMR (e.g. B213), as the bridge identification symbol (Table 6), as was used in previous studies (e.g. Isakovic and Fischinger, 2006; Casarotti and Pinho,

2006; Isakovic et al., 2008). In this arrangement, the letter B stands for the word ‘Bridge’ and the letters L, M and R represent the scale number for each of the three piers (left, middle and right) normalized with

respect to the short pier length (i.e. 7 m). Thus, the bridge B213 (the reference bridge) has the left pier of 14 m, the middle pier of 7 m and the right pier of 21 m high.

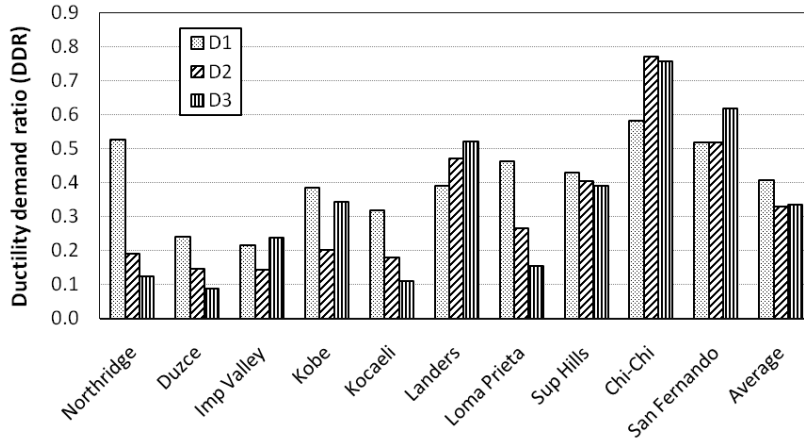


Fig. 14. Ductility demand ratio of the short pier for various design approaches

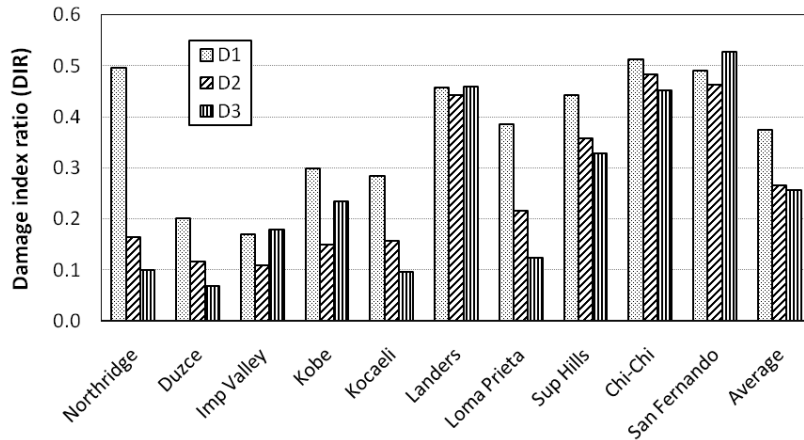


Fig. 15. Damage index ratio of the short pier for various design approaches

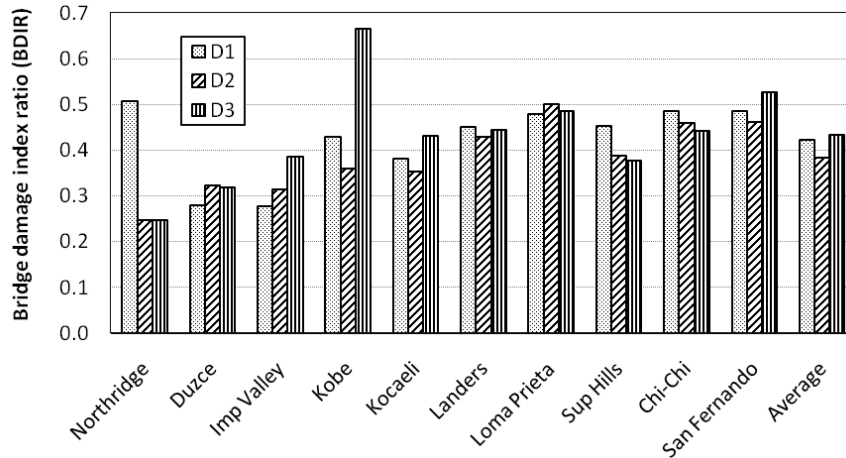
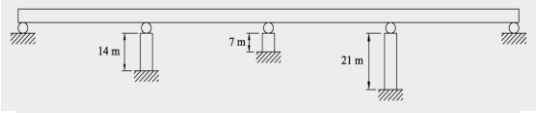
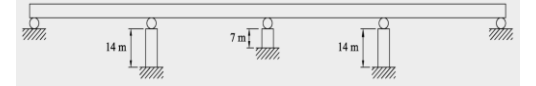
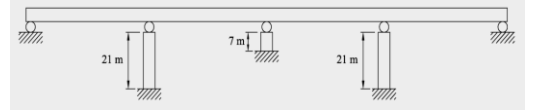


Fig. 16. Bridge damage index ratio for various design approaches

Table 5. SMA cross-sectional area for different design procedures

Design Procedure	SMA Ultimate Strain (%)	SMA Stress at Ultimate Strain (Mpa)	SMA Cross Sectional Area (mm ²)
D1	6.00	580	10029
D2	6.50	880	6793
D3	7.00	1180	5027

Table 6. Bridge configurations considered for the study of irregularity effects

Bridge Label	Left Pier Height (m)	Middle Pier Height (m)	Right Pier Height (m)	Configuration
B213	14	7	21	
B212	14	7	14	
B313	21	7	21	

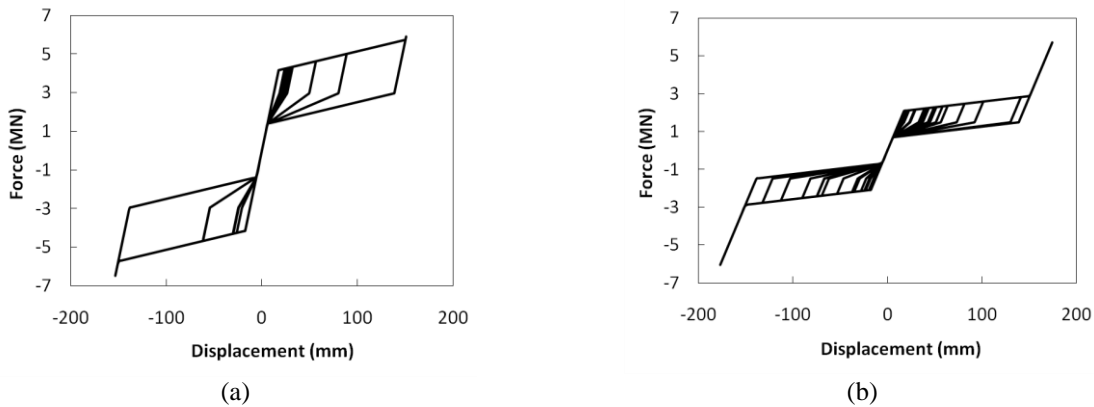


Fig. 17. Force-displacement relationship of the SMA elements for the Superstition Hills' earthquake: a) 6% strain, b) 7% strain

Figures 18-20 compare DDR and DIR of the short pier and BDIR, respectively, for bridges with different configurations under the suite of ground motions. The results are obtained for an $L_{SMA} = 2500$ mm, short pier reinforcement ratio of 2%, and ultimate design strain of 6% for the SMA elements. The degree of effectiveness varies from one record to another. In particular, in the cases of Northridge, Kobe and Kocaeli, the SMA devices perform better for the highly irregular bridge (B313), while in the cases of the Landers, Chi-Chi and San Fernando records, the SMA devices were more effective for the reference bridge (B213) and the bridge with

the lower degree of irregularity (B212). However, on average, the level of improvement is similar for the different bridge configurations (Figure 21), with increasing the bridge irregularity. On average, the SMA devices dissipate 41%, 48% and 52% of total hysteretic energy for bridge configurations of B212, B213 and B313, respectively. This is most likely due to the fact that, in the highly irregular bridge, there is more concentration of the ductility and energy demand on the short pier, which makes the SMA devices participate more in energy dissipation for that configuration.

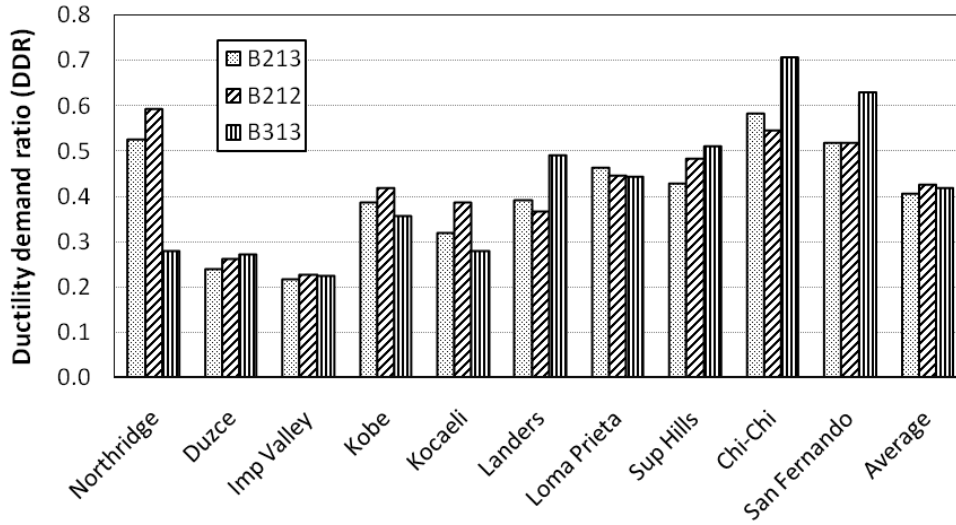


Fig. 18. Ductility demand ratio of the short pier for various bridge configurations

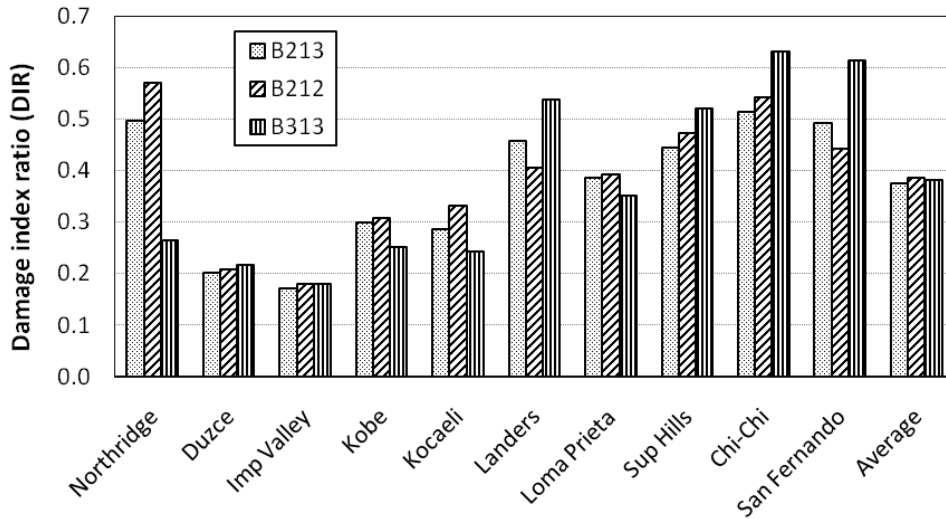


Fig. 19. Damage index ratio of short pier for various bridge configurations

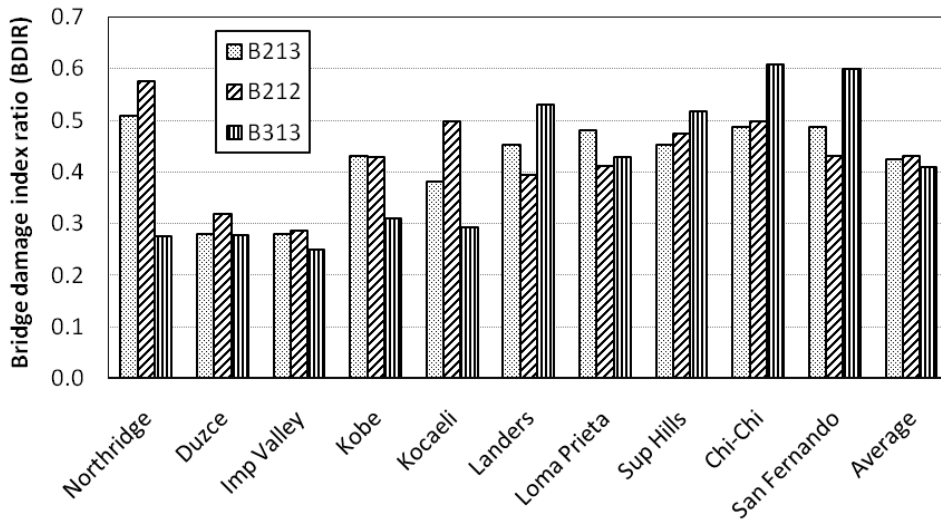


Fig. 20. Bridge damage index ratio for various bridge configurations

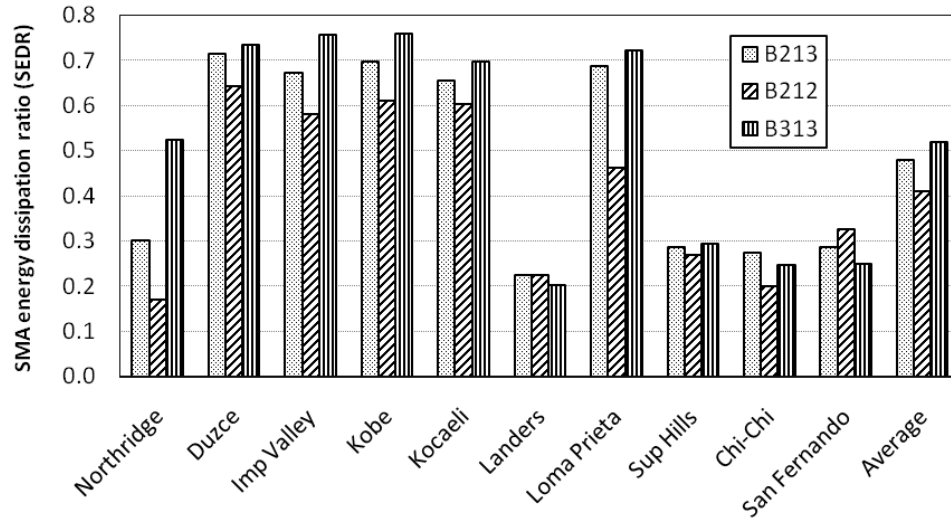


Fig. 21. Energy dissipation ratio for various bridge configurations

CASE STUDY

In order to provide a better understanding of the behavior of the SMA devices used at the short pier connection, a case study was conducted using the 1994 Northridge earthquake record for the reference bridge (B213), with $L_{SMA} = 2500$ mm, $\rho = 2\%$ for the short pier, and design ultimate strain of 6% for the SMA elements.

Figure 22 displays time histories of the deck and short pier displacement for the retrofitted bridge and the reference bridge. Although the maximum deck displacement does not change dramatically, the SMA devices reduce the maximum short pier displacement significantly from 332 mm to 183 mm (i.e. 45% reduction in the short pier ductility demand). This decrease in the short central pier ductility demand without a notable change in the ductility demand of the medium and long piers leads to a more balanced distribution of the ductility demand on the bridge piers. Also, residual deck displacement at the end of the motion decreases from 45 mm to 20 mm (mostly due to the re-centering capability of the SMA devices). However, implementation of the SMA devices on just one pier is not sufficient for restoring the residual displacement

completely.

Force-displacement relationships of the short pier in the reference bridge, as well as the SMA-controlled bridge, are illustrated in Figure 23. The wider hysteresis of the short pier in the reference bridge when compared to the retrofitted bridge represents a considerably larger amount of hysteretic energy dissipation. This higher amount of hysteretic energy results in a larger damage index for the reference bridge (e.g. in this case study, the damage index of the short pier exceeded 1.0 meaning that the pier would collapse under that ground motion). However, in the retrofitted bridge, the SMA devices provide additional energy dissipation capacity and control the damage in the short pier (i.e. the short pier damage index is reduced to 0.5). To give a clearer understanding of the effectiveness of the SMA elements in controlling the damage of the short pier, time histories of the total hysteretic energy and energy absorbed by subcomponents of the bridge are plotted in Figure 24. The absorbed energy in the reference bridge is concentrated in the short middle pier, which dissipates more than 80% of the total hysteretic energy, while the medium and long piers jointly can dissipate only 20% of the total hysteretic energy. This

inconsistent distribution of energy demand on different piers highlights the influence of irregularity on the seismic behavior of the bridge. However, in the retrofitted bridge, the energy is dissipated mainly by the short pier and the SMA devices. Specifically, the short pier and SMA devices dissipate 44% and 30% of the total hysteretic energy, respectively; while the medium and long piers jointly dissipate 26% of the total hysteretic energy. These results show that the retrofitting technique is successful in balancing the energy demand on different piers and regularizing the behavior of the bridge.

The proposed method is also successful in balancing the stiffness of adjacent bents. Equivalent stiffness of the middle bent can be calculated by considering the SMA device and the short pier as two structural elements in series. The stiffness ratio of the adjacent bents between the left and middle bents and the middle and right bents are estimated to be 1.3 and 2.5, respectively. Since AASHTO specifications suggest a bent stiffness ratio of 4 as the borderline of regularity for four-span bridges, the retrofitted bridge is now considered to be regular from a stiffness perspective.

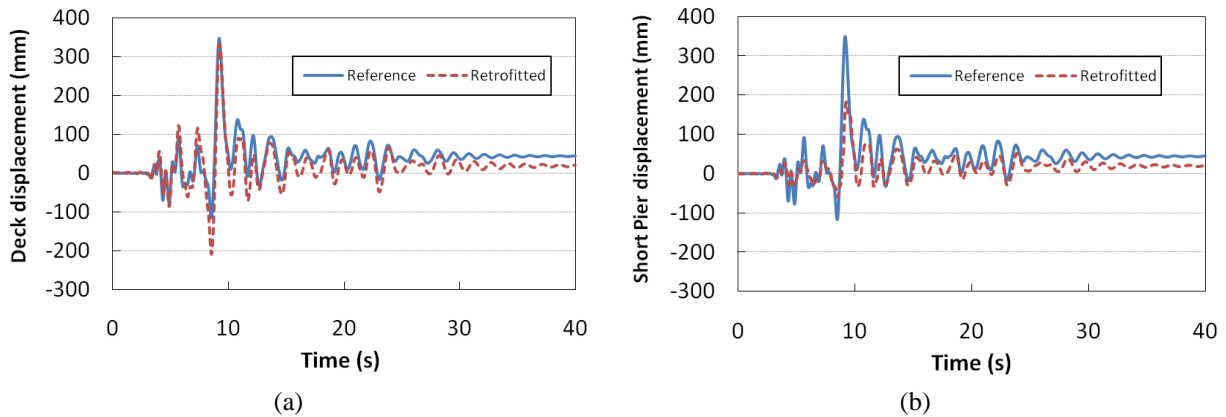


Fig. 22. Time histories of the deck and the short pier displacement in the retrofitted and reference bridges: a) Deck displacement, b) Short Pier displacement

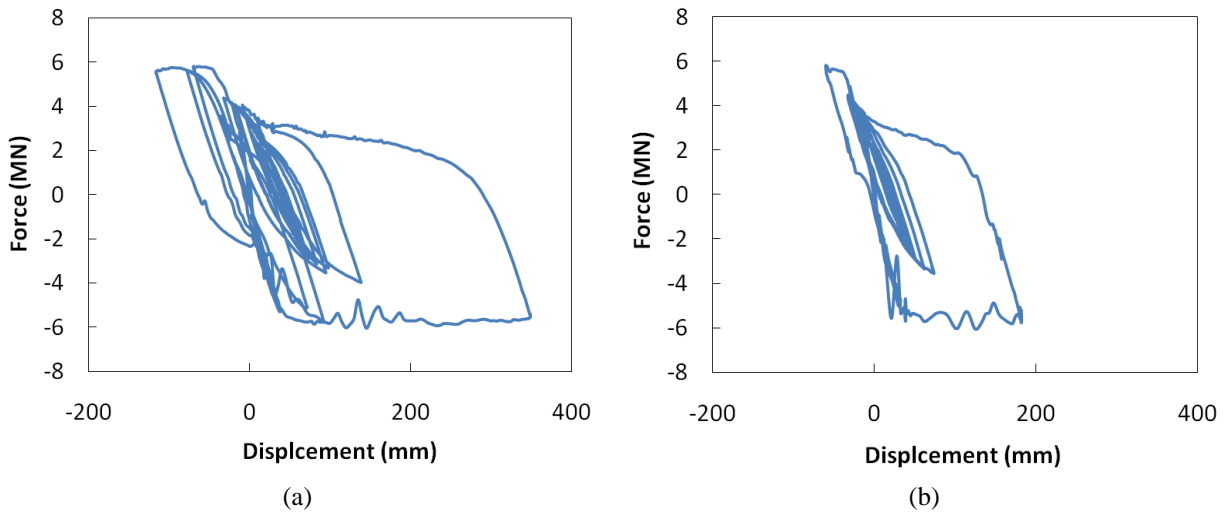


Fig. 23. Force-displacement relationships of the short pier in the reference and retrofitted bridges: a) Reference bridge, b) Retrofitted bridge

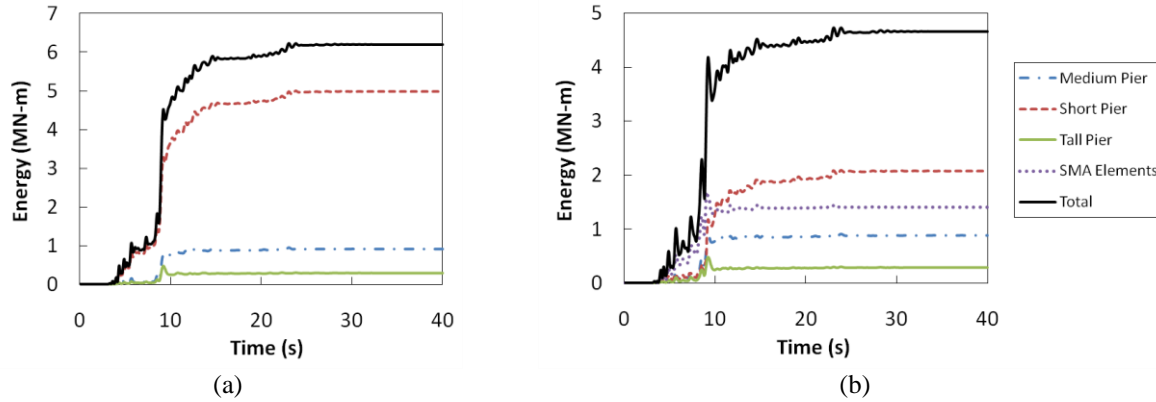


Fig. 24. Time histories of the total hysteretic energy and energy absorbed by sub-components, a) Reference bridge, b) Retrofitted bridge

DISCUSSION AND CONCLUSIONS

The effectiveness of the proposed method is investigated by comparing the seismic behavior of a SMA-controlled bridge and the reference bridge through parametric and case studies. The proposed method is an innovative approach in which the vulnerability to collapse is limited and tends to improve the seismic behavior of the irregular bridges. This method possesses advantages over other techniques for balancing the stiffness of adjacent bents. One of these techniques uses only a sliding bearing at the top of the short pier. This method eliminates the ductility demand on the short pier but significantly decreases the stiffness of structure, as the short pier is the stiffest element of the structure. This would then require excessive ductility demands on the other piers and high displacement demands on the bearings, thereby making the bridge vulnerable to collapse. Adding SMA bars to the sliding bearing compensates the reduction in stiffness and avoids excessive ductility demands on medium and tall piers. In addition, SMA elements provide reliable energy dissipation due to their “flag shape” hysteresis loops. Another technique for balancing pier stiffness in irregular bridges is adding a preshaft or increasing the effective height of the shorter piers. However, this technique is expensive and hard to apply,

while the proposed method is simple and easily applicable.

In regular bridges, ductility demand distribution is somewhat uniform among piers. However, construction of irregular bridges with different pier heights, especially in mountainous areas, is sometimes inevitable. This innovative technique regularizes the ductility demand on piers in irregular bridges with different pier heights and avoids excessive ductility demands on the short pier. Additionally, SMA devices have the benefit of being tunable for balanced stiffness of adjacent bents usually seen in regular bridges through modification of their geometries.

In this research, an analytical study was conducted to evaluate the effectiveness of shape memory alloy devices in improving the seismic behavior of irregular bridges. An irregular single column bent highway viaduct with unequal pier heights was modeled and utilized as a reference bridge. A pushover analysis on the reference bridge revealed a highly, non-uniform distribution of ductility demand due to irregularities in pier stiffnesses. As a retrofitting technique, the fixed bearing at the top of the short pier was replaced by a low-friction, sliding bearing and two groups of SMA elements. The cross-sectional area of the SMA elements was designed to keep the maximum strain of the SMA devices within the recoverable strain

range. The seismic behavior of the SMA-controlled bridge was compared with that of a reference bridge through parametric and case studies using a suite of ten ground motion records. The parameters for the analysis were chosen to be the length of SMA devices, the short pier reinforcement ratio (which corresponds to different cross-sectional areas of the SMA elements), the ultimate design strain of the SMA elements, and the height of the medium and long piers (degree of irregularity). Time-history analyses were conducted to assess the effects of these parameters on the various evaluation indices of the bridge. In particular, evaluation indices included the ductility demand ratio, damage index ratio, and SMA energy dissipation ratio of the retrofitted bridge in a normalized format in relation to the reference bridge responses.

Although the ductility demand ratio (DDR) and damage index ratio (DIR) of the medium and long piers increased slightly with the length of SMA devices (L_{SMA}), the DDR and DIR of the short pier and bridge damage index ratio (BDIR) continuously decreased for increasing values of L_{SMA} , until the L_{SMA} exceeded 2500 mm, at which point improvement noticeably slowed. Therefore, the optimum length of the SMA device can be considered to be 2500 mm. The results showed that for $L_{SMA} = 2500$ mm, there were average decreases of 56% and 63% in the ductility demand and damage index of the short pier, respectively compared to the responses of the reference bridge, which lead to a 55% reduction in average bridge damage index across the 10 excitation cases. Also, the variation of the short pier reinforcement ratio (ρ), which corresponds to a change in the cross-sectional area of SMA elements, does not significantly change the peak response quantities. However, on average, the SMA devices are more effective in reducing the response of the structure in the case of $\rho = 2\%$.

The effect of ultimate design strain of the SMA elements was also investigated by changing the design procedure. Those results showed that the SMA devices designed for an ultimate strain of 6.5% and 7% exhibit similar or even better performance than the SMA devices designed for an ultimate strain of 6%. Since increasing the design ultimate strain corresponds to a decrease in the cross-sectional area of the SMA elements, this result can lead to significant savings in the volume of SMA material needed for the retrofitting technique.

Finally, the effectiveness of the SMA devices for different degrees of bridge irregularity was investigated. On the average, for ten different seismic excitation levels the improvement is similar. In most records, the SMA devices contribute more in energy dissipation with increasing bridge irregularity. On average, the SMA devices dissipated 41%, 48% and 52% of the total hysteretic energy for bridge configurations of B212, B213 and B313, respectively.

REFERENCES

- Alvandi, S. and Ghassemieh, M., (2014), "Seismic evaluation of base isolated system equipped with Shape memory alloys", *Advanced Materials Research*, 831, 110-114.
- American Association of State Highway and Transportation Officials (2007). *AASHTO, AASHTO LRFD Bridge Design Specifications*, Washington, DC.
- Aryan, H. and Ghassemieh, M., (2014). "Mitigation of vertical and horizontal seismic excitations on bridges utilizing shape memory alloy system", *Advanced Materials Research*, 831, 90-94.
- Aryan, H. and Ghassemieh, M. (2015). "Seismic enhancement of multi-span continuous bridges subjected to three-directional excitations", *Smart Materials and Structures*, 24(4), 45030.
- Aryan, H. and Ghassemieh, M. (2017). "A superelastic protective technique for mitigating the effects of vertical and horizontal seismic excitations on highway bridges", *Journal of Intelligent Material Systems and Structures*, 28(12), 1533-1552.
- Baker, J.W., Lin, T., Shahi, S.K. and Jayaram, N. (2011). *New ground motion selection procedures and selected motions for the PEER transportation*

- research program, Pacific Earthquake Engineering Research Center.
- Brocca, M., Brinson, L.C. and Bazant, Z.P. (2002). “Three-dimensional Constitutive Model for Shape Memory Alloys Based on Microplane Model”, *Journal of Mechanics and Physics of Solids*, 50, 1051-1077.
- Calvi, G.M. and Pinto, P.E. (1994). “Seismic design of bridges: experimental and analytical research”, *Proceedings of the 10th European Conference on Earthquake Engineering*, pp. 2899-2904.
- Farmani, M.A. and Ghassemieh, M. (2016). “Shape memory alloy-based moment connections with superior self-centering properties”, *Smart Materials and Structures*, 25(7), 075028.
- Farmani, M.A. and Ghassemieh, M. (2017). “Steel beam-to-column connections equipped with SMA tendons and energy dissipating devices including shear tabs or web hourglass pins”, *Journal of Steel Construction Research*, 135, 30-48.
- Federation Internationale du Beton (FIB) (2007). *Seismic bridge design and retrofit—structural solutions*, FIB Bulletin 39.
- FEMA (2009), *Quantification of Building Seismic Performance Factors (FEMA P-695)*. Prepared by the Applied Technology Council for the Federal Emergency Management Agency Washington, DC.
- Ghassemieh, M., Bahari, M.R., Ghodrati, S.M. and Nojumi, S.A. (2012). “Improvement of concrete shear wall structures by smart materials”, *Open Journal of Civil Engineering*, 2, 87-95.
- Ghassemieh, M., Ghodrati, S.M., Bahari, M.R. and Nojumi, S.A. (2013). “Seismic enhancement of coupled shear walls using shape memory alloys”, *Journal of Civil Engineering and Science*, 2(2), 93-101.
- Ghassemieh, M., Mostafazadeh, M. and Sadeh, M.S. (2012). “Seismic control of concrete shear wall using shape memory alloys”, *Journal of Intelligent Material Systems and Structures*, 23(5), 535-543.
- Ghassemieh, M., Rezapour, M. and Sadeghi, V. (2017). “Effectiveness of the shape memory alloy reinforcement in concrete coupled shear walls”, *Journal of Intelligent Material Systems and Structures*, 28(5), 640-652.
- Guo, A., Zhao, Q. and Li, H. (2012). “Experimental study of a highway bridge with shape memory alloy restrainers focusing on the mitigation of unseating and pounding”, *Earthquake Engineering and Engineering Vibration*, 11(2), 195-204.
- Han, Y.L., Yin, H.Y., Xiao, E.T., Sun, Z.L. and Li, A.-Q. (2006). “A kind of NiTi-wire shape memory alloy damper to simultaneously damp tension, compression and torsion”, *Structural Engineering and Mechanics*, 22(2), 241-262.
- Isaković, T. and Fischinger, M. (2006). “Higher modes in simplified inelastic seismic analysis of single column bent viaducts”, *Earthquake engineering & structural dynamics*, 35(1), 95-114.
- Isaković, T., Lazaro, M.P.N. and Fischinger, M. (2008). “Applicability of pushover methods for the seismic analysis of single-column bent viaducts”, *Earthquake Engineering and Structural Dynamics*, 37(8), 1185-1202.
- Johnson, R., Padgett, J.E., Maragakis, M.E., DesRoches, R. and Saiidi, M.S. (2008). “Large scale testing of nitinol shape memory alloy devices for retrofitting of bridges”, *Smart Materials and Structures*, 17(3), 035018.
- Kappos, A.J., Manolis, G.D. and Moschonas, I.F. (2002). “Seismic assessment and design of R/C bridges with irregular configuration, including SSI effects”, *Engineering Structures*, 24(10), 1337-1348.
- McKenna, (2011). “OpenSees: a framework for earthquake engineering simulation”, *Computing in Science and Engineering*, 13(4), 58-66.
- Motahari, S.A., Ghassemieh, M. and Abolmaali, S.A. (2007). “Implementation of shape memory alloy dampers for passive control of structures subjected to seismic excitations”, *Journal of Constructional Steel Research*, 63(12), 1570-1579.
- Ozbulut, O.E. and Hurlbaas, S. (2011). “Seismic assessment of bridge structures isolated by a shape memory alloy/rubber-based isolation system”, *Smart Materials and Structures*, 20(1), 015003.
- Pinto, A.V., Verzeletti, G., Magonette, G., Pegon, P., Negro, P. and Guedes, J. (1996). “Pseudo-dynamic testing of large-scale R/C bridges in ELSA”, *11th World Conference on Earthquake Engineering*, pp. 23-28.
- Roh, H., Reinhorn, A.M. and Lee, J.S. (2012). “Modeling and cyclic behavior of segmental bridge column connected with shape memory alloy bars”, *Earthquake Engineering and Engineering Vibration*, 11(3), 375-389.
- Saiidi, M.S. and Wang, H. (2006). “Exploratory study of seismic response of concrete columns with shape memory alloys reinforcement”, *ACI Structural Journal*, 103(3), 436-443.
- Sharabash, A.M. and Andrawes, B.O. (2009). “Application of shape memory alloy dampers in the seismic control of cable-stayed bridges”, *Engineering Structures*, 31(2), 607-616.
- Shrestha, K.C., Araki, Y., Nagae, T., Omori, T., Sutou, Y., Kainuma, R. and Ishida, K. (2011). “Applicability of Cu-Al-Mn shape memory alloy bars to retrofitting of historical masonry constructions”, *Earthquakes and Structures*, 2(3), 233-256.